Vol 18 No 4, April 2009
1674-1056/2009/18(04)/1503-09

Chinese Physics B

© 2009 Chin. Phys. Soc.
and IOP Publishing Ltd

Hybrid method for investigation of electromagnetic scattering from conducting target above the randomly rough surface*

Wang Rui(王 蕊)†, Guo Li-Xin(郭立新), Ma Jun(麻 军), and Wu Zhen-Sen(吴振森)

School of Science, Xidian University, Xi'an 710071, *China*

(Received 9 January 2008; revised manuscript received 10 November 2008)

A current based hybrid method (HM) is proposed which combines the method of moment (MOM) with the Kirchhoff approximation (KA) for the analysis of scattering interaction between a two-dimensional (2D) infinitely long conducting target with arbitrary cross section and a one-dimensional (1D) Gaussian rough surface. The electromagnetic scattering region in the HM is split into KA region and MOM region. The electric field integral equation (EFIE) in MOM region (target) is derived, the computational time of the HM depends mainly on the number of unknowns of the target. The bistatic scattering coefficient for the infinitely long cylinder above the rough surface with Gaussian roughness spectrum is calculated, and the numerical results are compared and verified with those obtained by the conventional MOM, which shows the high efficiency of the HM. Finally, the influence of the size, location of the target, the rms height and correlation length of the rough surface on the bistatic scattering coefficient with different polarizations is discussed in detail.

Keywords: method of moment, hybrid method, Gaussian rough surface, bistatic scattering

PACC: 4120, 4110H

1. Introduction

Electromagnetic scattering from the target above a rough surface has attracted much interest during recent years because of its importance in such topic in radar surveillance, target tracking, and oceanic remote sensing. The study of such electromagnetic scattering model is a complex and difficult subject due to the difficulty in calculating the coupling scattering between the target and the rough surface, so most scattering models developed previously for this problem are based on single scattering properties of the scatterers, and in these models, the scattering interaction between the target and the rough surface is ignored. Up to now, the methods to solve this problem are mainly of two kinds, one of which is based on some approximate method, such as the Kirchboff approximation (KA), the image technique and the extended boundary condition method;[1,2] the other includes some numerical methods[3−7] based on method of moment (MOM), EFIE (electric field integration equation) / MFIE (magnetic field integral equation) / CFIE (combined field integral equation), FDTD (finite difference time-domain), FEM (finite element method) / BEM (boundary element method) which have been used to obtain the exact solution in problems of calculating the electromagnetic scattering from a target lying above a rough surface, such as generalized forward-backward method, spectrum acceleration arithmetic, finite element method and domain decomposition method. A well-known fact is that the advantage of the approximate method is high efficiency and its disadvantage is low precision because of the calculation of the coupling scattering; whereas the numerical method has high precision and low efficiency. To overcome the disadvantage of both approximate and numerical methods, recent relevant works about the scattering behaviour of targets above rough surfaces include kinds of hybrid algorithm such as the analytical solution combining KA and reciprocity which is discussed by Chiu *et al*[8] for the case of predicting the near-field interaction between a dielectric cylinder and a slightly rough surface. Ye Jin[9] and Johnson[10] studied the difference field radar cross sec-

*Project supported by the National Natural Science Foundation of China (Grant No 60571058), the Specialized Research Fund for the Doctoral Program of Higher Education, China.

†E-mail: doufuruier@yahoo.cn

tion from the target above a rough surface by FBM–CGM (forward-backward method-conjugate gradient method). Wang *et al*[11] used the reciprocity theorem to study the electromagnetic scattering interaction between a perfect conducting plate and a one-dimensional conducting slightly rough surface. In this paper, a new hybrid algorithm combining MOM with KA is proposed. The KA is used for the calculation of the Gaussian rough surface and MOM for the target. The coupling scattering is mapped to change the matrix elements in the calculation of MOM. So the HM includes completely all the coupling interactions between the rough surface and the target. Moreover, KA has been an efficient method to calculate the scattering from the rough surface, hence, the results obtained by the HM that allows of a substantial reduction of computational time and memory requirements are in reasonable agreement with those based on the application of the conventional MOM. The paper is organized as follows: the theoretical formulation of HM is developed in Section 2, and numerical results about the scattering coefficient of the composite model are given and discussed in Section 3. Section 4 gives the conclusions and the future investigation in this topic.

2. Hybrid method in the scattering model

For the scattering computation, surface realizations are needed at a set of P points with spacing Δx over a length of $L = P\Delta x$. Realizations with the desired properties can be generated at points $x_p = p\Delta x$ $(p = 1, ..., P)$ using

$$f(x_p) = \frac{1}{L}\sum_{i=-\frac{P}{2}}^{\frac{P}{2}-1} F(K_i)\exp(jK_i x_p), \tag{1}$$

where, for $i \geq 0$,

$$F(K_i) = \sqrt{2\pi LW(K_i)}\begin{cases} [N(0,1) + jN(0,1)]/\sqrt{2} & i \neq 0, \quad P/2; \\ N(0,1) & i = 0, \quad P/2; \end{cases} \tag{2}$$

and, for $i < 0$, $F(K_i) = F(K_{-i})^*$ with $K_i = 2\pi i/L$, and each time $N(0,1)$ appears, which indicates an independent sample taken from a zero mean, unit variance Gaussian distribution. For the present work, the rough surface used in scattering model is generated randomly with a Gaussian roughness spectrum,[12] i.e.

$$W(K_i) = (l\delta^2/2\sqrt{\pi})\mathrm{e}^{-K_i^2 l^2/4}, \tag{3}$$

where δ denotes the rms height and l is the correlation length. Equation (1) is computed with a fast Fourier transform.

As we have already known, MOM is a popular numerical algorithm with high accuracy. For the less number of unknowns, common computers can often meet the computational time and memory requirements of MOM. However, with the increase of the number of unknowns, the size of the system of linear equations becomes larger promptly. For example, to solve the problem of calculating scattering coefficient of the electromagnetic scattering from the composite model for the target lying above the large-scale rough surface, the computational requirements of MOM may exceed the available computational capacities. The HM proposed in this section, combining MOM with KA, mainly aims at decreasing the number of unknowns by MOM, which is described in the following.

Consider an incident wave $\psi^{\mathrm{in}}(\boldsymbol{r})$ impinging upon a target and a randomly rough surface with height profile $y = f(x)$ (Fig.1). In 2D scattering problem $\boldsymbol{r} = x\hat{\boldsymbol{x}} + y\hat{\boldsymbol{y}}$, the incident wave vector is

$$\boldsymbol{k} = k(\hat{\boldsymbol{x}}\sin\theta_i - \hat{\boldsymbol{y}}\cos\theta_i). \tag{4}$$

As shown in Fig.1, the scattering region of the 2D composite model is split into MOM region (for target) and KA region (for rough surface). In principle, this subdivision can be performed in an arbitrary manner. In practice, in order to reduce the number of unknowns by MOM as possible, the target should be divided into the MOM region and the larger-scale rough surface be divided into the KA region. Here, the target is subdivided into N segments and the rough surface P segments.

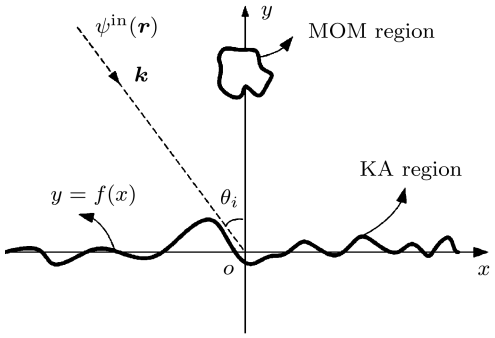


Fig.1. Composite model of a 2D target above the rough surface.

In this paper, both the induced current densities of the MOM and KA regions are expressed as linear superposition of pulse basis functions, i.e.

$$\boldsymbol{J}^{\rm MOM}=\sum_{n=1}^{N}\alpha_n\boldsymbol{f}_n, \tag{5}$$

$$\boldsymbol{J}^{\rm KA}=\sum_{p=1}^{P}\beta_P\boldsymbol{f}_P. \tag{6}$$

The scattered fields due to the currents can be expressed as

$$\boldsymbol{E}^s=\boldsymbol{L}^e(\boldsymbol{J}), \tag{7}$$

$$\boldsymbol{H}^s=\boldsymbol{L}^h(\boldsymbol{J}), \tag{8}$$

where $\boldsymbol{L}^e$ and $\boldsymbol{L}^h$ are defined respectively as[13]

$$\boldsymbol{L}^e(\boldsymbol{J})=-j\omega\mu\int_{\Gamma}\left(\overline{\overline{I}}+\frac{\nabla\nabla'}{k^2}\right)\cdot\boldsymbol{J}(\boldsymbol{r}')g(\boldsymbol{r},\boldsymbol{r}')\mathrm{d}\Gamma', \tag{9}$$

$$\boldsymbol{L}^h(\boldsymbol{J})=\nabla\times\int_{\Gamma}\boldsymbol{J}(\boldsymbol{r}')g(\boldsymbol{r},\boldsymbol{r}')\mathrm{d}\Gamma'. \tag{10}$$

Here $\overline{\overline{I}}$ is the unit dyad and the 2D Green's function $g(\boldsymbol{r},\boldsymbol{r}')=\dfrac{1}{4j}H_0^{(2)}(k\,|\boldsymbol{r}-\boldsymbol{r}'|)$. In contrast to the MOM coefficients α_n, the KA coefficients β_p are not based on the solution of a system of linear equations, but they are obtained through an application of the KA. Equation (6) leads to a very efficient and flexible HM. In the KA region (rough surface), using KA ($kl>6,\ l^2>2.76\delta\lambda$), the scattered field of the rough surface can be obtained as[14]

$$\boldsymbol{E}^s(\boldsymbol{r})=-j\omega\mu\int_{\Gamma}\left(\overline{\overline{I}}+\frac{\nabla\nabla'}{k^2}\right)\cdot2\hat{\boldsymbol{n}}\times\boldsymbol{H}^{\rm in}(\boldsymbol{r}')\,g(\boldsymbol{r},\boldsymbol{r}')\mathrm{d}\Gamma', \tag{11}$$

where $\boldsymbol{H}^{\rm in}$ denotes the incident magnetic fields and $\hat{\boldsymbol{n}}$ represents the normal vector of the rough surface contour. From Eqs.(7), (9) and (11), the current $\boldsymbol{J}^{\rm KA}$ is acquired by KA as

$$\boldsymbol{J}^{\rm KA}(\boldsymbol{r})=2\hat{\boldsymbol{n}}\times\boldsymbol{H}^{\rm in}(\boldsymbol{r}). \tag{12}$$

The conventional KA current density is solely determined by $\boldsymbol{H}^{\rm in}$ as shown in Eq.(12) without the existence of the target, however, for the composite model, the influence of the target (MOM region) above the rough surface must be considered as well. Thus taking into account the influence of $\boldsymbol{J}^{\rm MOM}$ (MOM region), the modification of Eq.(12) can be rewritten as[13]

$$\boldsymbol{J}^{\rm KA}(\boldsymbol{r})=2\hat{\boldsymbol{n}}\times\boldsymbol{H}^{\rm in}(\boldsymbol{r})+2\hat{\boldsymbol{n}}\times\boldsymbol{L}^h\left(\sum_{n}^{N}\alpha_n\boldsymbol{f}_n\right). \tag{13}$$

The first term on the right-hand side of Eq.(13) still represents the conventional KA current density due to the incident magnetic field $\boldsymbol{H}^{\rm in}$. In Eq.(13), a summation takes place over basis function $\boldsymbol{f}_n$ in the MOM region with coefficients α_n. The operator $\boldsymbol{L}^h$ acting on $\boldsymbol{f}_n$ yields the magnetic field strength due to the basis functions. The vector product $2\hat{\boldsymbol{n}}\times$ gives the additional KA current density. Thus, by comparing Eq.(13) with Eq.(6), the coefficients β_p can be obtained as

$$\beta_p=\left[2\hat{\boldsymbol{n}}\times\boldsymbol{H}^{\rm in}(\boldsymbol{r}_p)\cdot\boldsymbol{f}_p+\sum_{n}^{N}\alpha_n2\hat{\boldsymbol{n}}\times\boldsymbol{L}^h(\boldsymbol{f}_n)\cdot\boldsymbol{f}_p\right]. \tag{14}$$

For the horizontal polarization of electromagnetic scattering,

$$\beta_p=\left[2\hat{\boldsymbol{n}}\times\boldsymbol{H}^{\rm in}(\boldsymbol{r}_p)\cdot\hat{\boldsymbol{z}}+\sum_{n}^{N}\alpha_n2\hat{\boldsymbol{n}}\times\boldsymbol{L}^h(\boldsymbol{f}_n)\cdot\hat{\boldsymbol{z}}\right]. \tag{15}$$

Inserting Eq.(15) into Eq.(6), we have

$$\boldsymbol{J}^{\rm KA}=\sum_{p=1}^{P}\left[2\hat{\boldsymbol{n}}\times\boldsymbol{H}^{\rm in}(\boldsymbol{r}_p)\cdot\hat{\boldsymbol{z}}+\sum_{n}^{N}\alpha_n2\hat{\boldsymbol{n}}\times\boldsymbol{L}^h(\boldsymbol{f}_n)\cdot\hat{\boldsymbol{z}}\right]\boldsymbol{f}_p. \tag{16}$$

For the 2D composite model, $\boldsymbol{E}=\hat{\boldsymbol{z}}E$ holds for the horizontal polarization of electromagnetic scattering and the $\hat{\boldsymbol{z}}$-component is the tangential component. Thus the total tangential electric field $\boldsymbol{E}$ is equal to zero according to the boundary condition, i.e.

$$\boldsymbol{E}=\left[\boldsymbol{E}^{\rm in}+\boldsymbol{E}^s\right]=0. \tag{17}$$

Here $\boldsymbol{E}^{\rm in}=\hat{\boldsymbol{z}}E^{\rm in}$ denotes the incident electric field. Application of the EFIE (17) in the MOM region leads to

$$\boldsymbol{L}^e\left[\sum_{n=1}^{N}\alpha_n\boldsymbol{f}_n\right]+\boldsymbol{L}^e\left[\sum_{p=1}^{P}\left[2\hat{\boldsymbol{n}}\times\boldsymbol{H}^{\rm in}(\boldsymbol{r}_p)\cdot\hat{\boldsymbol{z}}+\sum_{n}^{N}\alpha_n 2\hat{\boldsymbol{n}}\times\boldsymbol{L}^h(\boldsymbol{f}_n)\cdot\hat{\boldsymbol{z}}\right]\boldsymbol{f}_p\right]=-\boldsymbol{E}^{\rm in}. \tag{18}$$

Note that two different coupling mechanisms do exist between the KA and MOM regions. The currents in the MOM region contribute to the KA currents as expressed in Eq.(13), and in Eq.(18) the electric field radiated by the KA current must be taken into account when applying the boundary condition in the MOM region. Counterchanging p and n, we have

$$\sum_{n}^{N}\alpha_n\left[\boldsymbol{L}^e(\boldsymbol{f}_n)+\sum_{p=1}^{P}\left[(2\hat{\boldsymbol{n}}\times\boldsymbol{L}^h(\boldsymbol{f}_n)\cdot\hat{\boldsymbol{z}})\boldsymbol{L}^e(\boldsymbol{f}_p)\right]\right]=-\boldsymbol{E}^{\rm in}-\sum_{p=1}^{P}\left[(2\hat{\boldsymbol{n}}\times\boldsymbol{H}^{\rm in}(\boldsymbol{r}_p)\cdot\hat{\boldsymbol{z}})\boldsymbol{L}^e(\boldsymbol{f}_p)\right]. \tag{19}$$

By applying suitable weighting functions similar to the conventional MOM, the integral equation (19) can be converted into a system of linear equations for the N unknown coefficients α_n. Once the coefficients α_n have been determined, the coefficients β_p in Eq.(6) can be obtained from Eq.(15). After solving the current in the KA and MOM regions, respectively, the scattering field $\boldsymbol{E}^s$ could be directly calculated from Eq.(7), thus the scattering cross section is defined as[15]

$$\sigma_s(\theta_s)=\lim_{R\to\infty}2\pi R\frac{|E^s(R,\theta_s)|^2}{|E^{\rm in}|^2}. \tag{20}$$

It is necessary to point out that, in fact, the kernel of the HM presented above is a process to modify the original impedance and voltage matrix elements of the conventional MOM into a new matrix element. For example, equation (19) can be rewritten as

$$\sum_{n}^{N}\alpha_n\left[\boldsymbol{L}^e(\boldsymbol{f}_n)\right]+\sum_{n}^{N}\left(\alpha_n\sum_{p=1}^{P}\left[(2\hat{\boldsymbol{n}}\times\boldsymbol{L}^h(\boldsymbol{f}_n)\cdot\hat{\boldsymbol{z}})\boldsymbol{L}^e(\boldsymbol{f}_p)\right]\right)=-\boldsymbol{E}^{\rm in}-\sum_{p=1}^{P}\left[(2\hat{\boldsymbol{n}}\times\boldsymbol{H}^{\rm in}(\boldsymbol{r}_p)\cdot\hat{\boldsymbol{z}})\boldsymbol{L}^e(\boldsymbol{f}_p)\right]. \tag{21}$$

A set of weighting functions $\boldsymbol{w}_m$ is chosen. We can suppose that the quantity of the inner product of $\boldsymbol{w}_m$ and the first term on the left-hand side in Eq.(21) is the usual impedance matrix element $Z_{mn}=\langle\boldsymbol{w}_m,\boldsymbol{L}^e(\boldsymbol{f}_n)\rangle$ in conventional MOM. The quantity of the inner product of $\boldsymbol{w}_m$ and the second term on the left-hand side in Eq.(21) represent an additional field contribution to Z_{mn} that is also due to $\boldsymbol{f}_n$ that arrives at the observation point m by a physical process not directly accounted for in the MOM formulation. Thus, we may call it the Z^G_{mn},[16] where the superscript G denotes that Z^G_{mn} is an additional term added to, in general, each impedance matrix element due to a physical process G that also directs energy from the n-th basis current function $\boldsymbol{f}_n$ to the m-th observation point $\boldsymbol{f}_m$. Thus we may write for the new impedance matrix element

$$Z'=\left[Z_{mn}+Z^G_{mn}\right]. \tag{22}$$

The similar explanation is also applicable to the voltage matrix. Thus, the new voltage matrix can be written as

$$V'=\left[V_m+V^G_m\right], \tag{23}$$

where V^G_m is an additional term added to the original impedance matrix V_m when the incident wave arrives at the m-th observation point in a physical process not directly accounted for in the MOM formulation. Finally, the total Eq.(21) can be written as

$$\left[Z_{mn}+Z^G_{mn}\right]\left[\alpha_n\right]=\left[V_m+V^G_m\right], \tag{24}$$

V_m and V^G_m represent the first and second terms on the right-hand side of Eq.(21), respectively.

In fact, the analysis of the scattering for the composite model by the HM in this paper can be considered as a process to obtain the approximate expression of the strict Green function by KA. Thus the scattered fields obtained by the HM consider all the coupling interactions between the target and the rough surface, thus the numerical result is of high accuracy (shown in Section 3). In a word, it is based on the point of view to extend the conventional MOM using KA method. As for the vertical polarization of electromagnetic scattering with $\boldsymbol{H}^{\rm in}=\hat{\boldsymbol{z}}H^{\rm in}$ is concerned,

the relevant conclusion can be obtained in the similar way.

3. Numerical results and discussions

It should be noted that, in numerical simulations, the rough surface is truncated at $x = \pm L/2$. This means that the surface current is forced to be zero for $|x| > L/2$. If there is an abrupt change of surface current from nonzero to zero, artificial reflection from the two endpoints will occur. To avoid these problems, the tapered wave described by the tapering parameter g has been employed to guard against the edge effects. The tapered incident wave illuminating the composite model is given by[17]

$$\begin{aligned}&\psi^{\text{in}}(\boldsymbol{r})\\ &= \exp\left(-jk\left(x\sin\theta_i - y\cos\theta_i\right)\right.\\ &\quad \left.\times\left(1 + w\left(\boldsymbol{r}\right)\right)\right)\exp\left(-\left(\frac{x + y\,\text{tg}\,\theta_i}{g}\right)^2\right),\end{aligned} \tag{25}$$

where the incident wave $\psi^{\text{in}}(\boldsymbol{r})$ denotes $E^{\text{in}}(\boldsymbol{r})$ (for horizontal polarization) or $H^{\text{in}}(\boldsymbol{r})$ (for vertical polarization), θ_i is the incident angle. The additional factor in the phase, $w(\boldsymbol{r})$, is inserted such that ψ^{in} satisfies the wave equation to a higher order. The choice of $w(\boldsymbol{r})$ is expressed as[17]

$$w\left(\boldsymbol{r}\right) = \frac{\left[2\left(\dfrac{x + y\,\text{tg}\,\theta_i}{g}\right)^2 - 1\right]}{\left(kg\cos\theta_i\right)^2}. \tag{26}$$

As the basis of the tapered incident wave, the tapering parameter g and L at least should satisfy all requirements of the wave equation, correlation length, and energy truncation, giving[18]

$$g > \frac{6}{\cos\theta_i^{1.5}}, \tag{27}$$

$$L > 15l \quad \text{and} \quad L \geq 4g. \tag{28}$$

Moreover, to ensure that the target can be illuminated by the tapered wave adequately, the tapering parameter g should satisfy the following condition,

$$g = 4\left[\frac{r}{\cos\theta_i} + h\,\text{tg}\,\theta_i\right]. \tag{29}$$

For the purpose of taking into full consideration of interactions between the target and underlying surface, the truncated surface length L, which is related to the target size, height and the scattering angle, should satisfy

$$L \geq 2\left[\frac{r}{\cos\theta_{s,m}} + h\,\text{tg}\,\theta_{s,m}\right], \tag{30}$$

where $\theta_{s,m}$ is the maximal scattering angle, r is the maximal radius and h the distance of target away from the rough surface. The scattering geometry under the consideration is shown in Fig.2.

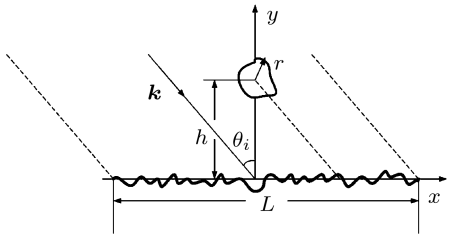


Fig.2. Scattering model of 2D target lying above the rough surface.

In order to examine the validity of the HM proposed in this paper, as an example, we first compute the bistatic scattering cross section of a 2D infinitely long cylinder above a Gaussian rough surface using the strict MOM and the HM, respectively. Both the relevant parameters of the target and rough surface are measured in incident wavelength λ, and the Gaussian rough surface is created by 50 Monte Carlo realizations in the following numerical simulations.

Figure 3 shows the bistatic scattering coefficient of a 2D perfectly electric conducting cylinder with radius λ and altitude $h = 3\lambda$ above a Gaussian rough surface with different rms height δ and correlation length l for both VV polarization [3(a) and 3(b)] and HH polarization [3(c) and 3(d)] using MOM (solid line) and the HM (dashed line). Here, the incident angles of the plots in Figs.3(a)–3(d) are 30°, 50°, 20°, 60°, respectively. It is found that the scattering pattern by the HM is in good agreement with that by the conventional MOM over the most angular scattering range for different incident angles and different polarizations, which indicates the validity of the HM proposed in this paper. Here, it is found that the scattering pattern obtained by our HM is not identical with that by MOM for the large scattering angle ($\theta_s > 70°$), which is caused by the limitations of the KA algorithm itself. Hence, it should be pointed out that our hybrid algorithm is applicable to the small and middle scattering angles. Since the computational time and memory requirements of

these two algorithms depend on the calculating conditions, which include the choice of the length of rough surface L (depending on the radius and location of the target), the δ and l of rough surface, the incident angles and the maximal scattering angle. Here we take Figs.3(a) and 3(b) for example, which give the comparison of the computational time and memory requirements by the HM and MOM, as shown in Table 1, where the spacing $\Delta x = \lambda/10$ and the lengths of the rough surface in Figs.3(a) and 3(b) are set to be 160λ and 240λ, respectively.

Table 1. Comparison of the computational time and memory requirements made by MOM and HM.

	method	computational time	ratio of the computational time by HM and MOM	memory requirements	ratio of memory requirements by HM and MOM
Fig.3(a)	MOM	190 s	7.9%	42 MB	2.8%
	HM	15 s		1.17 MB	
Fig.3(b)	MOM	720 s	3.2%	92 MB	1.9%
	HM	23 s		1.75 MB	

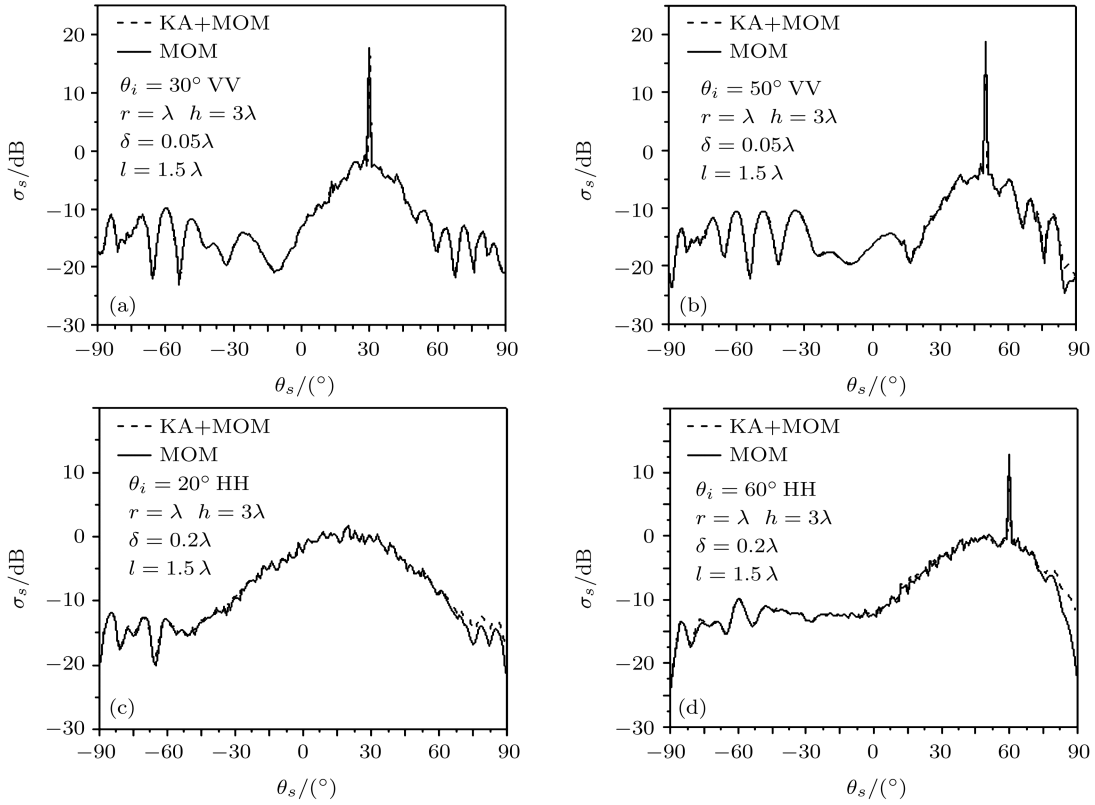


Fig.3. The bistatic scattering coefficient of a 2D perfectly electric conducting cylinder above a Gaussian rough surface impinged by a tapered wave with different polarization for different incident angles and different δ and l.

From Table 1, it is found that the HM in this paper shows a substantial reduction of computational time and memory requirements. Moreover, it can be found that the longer the rough surface (Fig.3(b)), the more the advantages the HM has as compared to the conventional MOM, which can also be seen from the ratio of the computation time and memory requirements by HM and MOM in Table 1. This result is mainly due to the fact that the size of the impedance matrix (determining the computational time and memory requirements) in HM is only determined by the number of the unknowns of the target.

To further explore the important scattering characteristics of the composite model, in Fig.4, the effect of the radius of cylinder r on the bistatic scattering coefficient of the cylinder above the rough surface is examined for different incident angles 30° and 60° (VV case). It is observed that the bistatic scattering coefficient of the composite model increases with increasing r for different incident angles. This is mainly due to the fact that the coupling scattered field increases as the coupling area between cylinder and surface becomes larger with the increase of r, resulting in the total bistatic scattering coefficient of composite model increases. Another point worth noting is that for the large incident angle, there is an obvious peak appearing on the specular direction in the total bistatic scattering coefficient. This is mainly caused by the strong scattering in the forward direction, in other words, once the incident angle becomes larger, the coupling area between the cylinder and surface becomes larger rapidly, because the coupling and the total scattered field on the specular direction will increase.

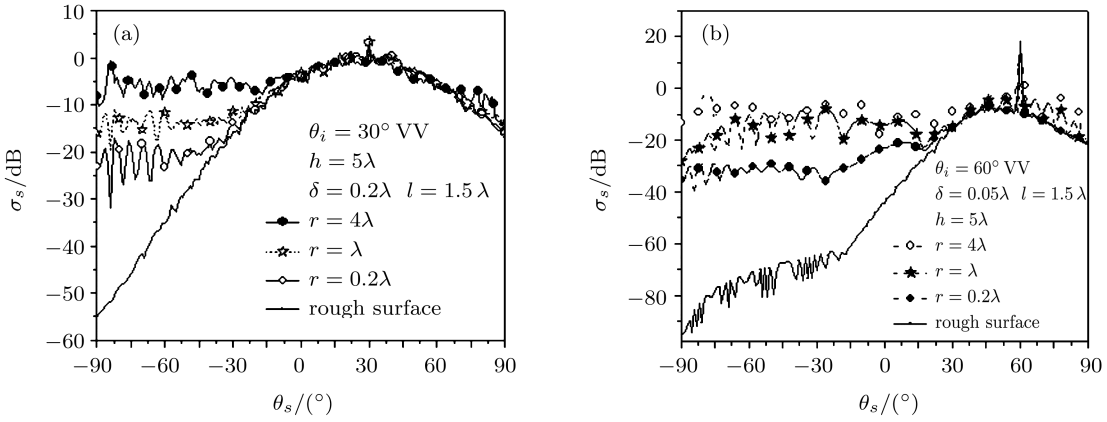


Fig.4. The bistatic scattering coefficient of the composite model versus r for different incident angles.

The dependency of the bistatic scattering coefficient on the altitude h of the cylinder is depicted for different polarizations in Fig.5. Here, the radius of the cylinder is λ, the rms height and the correlation length of the Gaussian rough surface are 0.2 and 1.5λ, respectively. It is shown that the amplitude of the bistatic scattering coefficient of the composite model is much greater than that of the rough surface only for most scattering angles except for the specular direction. This phenomenon is due to the fact that the contribution of the coupling scattered field to the total scattered field is small near the specular direction, thus the total bistatic scattering coefficient is not sensitive to the variation of h; whereas, the proportion of the coupling scattered field in the total scattered field becomes larger far from the specular direction, and a larger oscillation of the total scattered

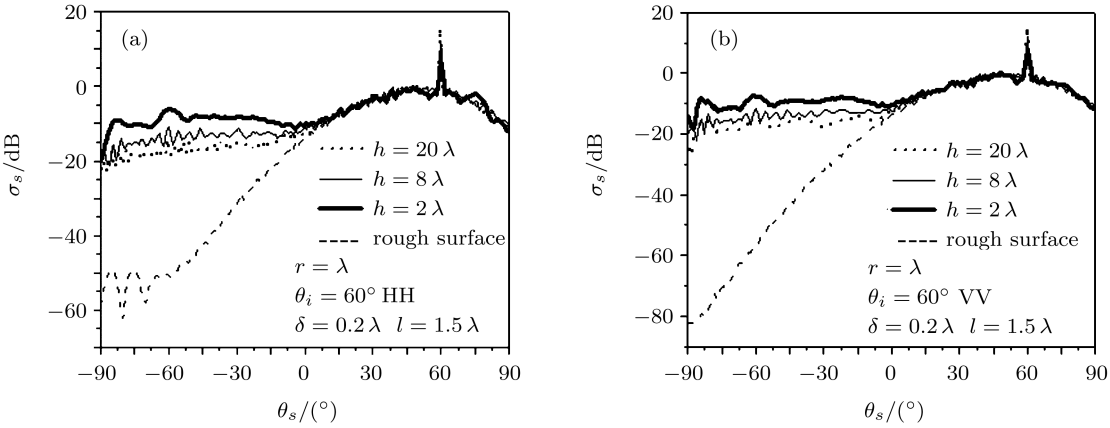


Fig.5. The bistatic scattering coefficient of the composite model versus h.

field is observed with the variation of h. However, the bistatic scattering coefficient of the composite model decreases at a gentler rate with the increase of h, which means that it is not sensitive to the variation of h.

In Fig.6, the influence of rms height δ of the Gaussian rough surface on the bistatic scattering coefficient of the composite model for the incident angle 30° in the VV case is also shown. It is observed that with the increase of δ, the bistatic scattering coefficient increases over the whole scattering region, especially near the specular direction. Moreover, there is an obvious peak in the specular direction for the smaller δ, which is due to the fact that with the same correlation length, the smaller the δ, the smoother the rough surface, and thus the more coherent scattered field appears in the specular direction. Figure 7 gives the dependence of correlation length l on the bistatic scattering coefficient for the incident angle 30° in the VV case. It can be found also that with the decrease of l, the bistatic scattering coefficient of the composite model increases obviously near the specular direction and then becomes almost identical far from the specular direction. As for the large l, the scattered field in the specular direction is visually large due to the contribution of the coherent component to the total scattered field becoming important.

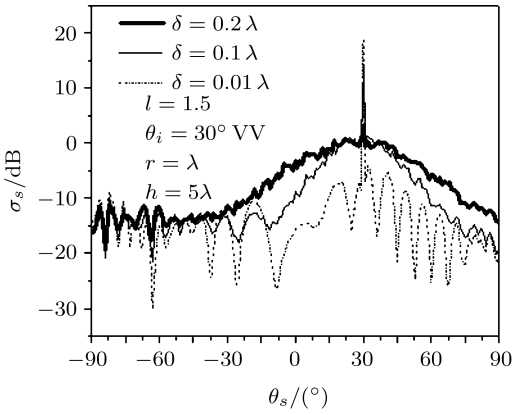


Fig.6. The bistatic scattering coefficient of the composite model versus δ.

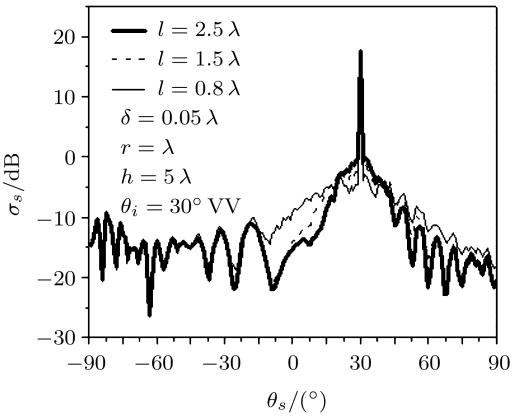


Fig.7. The bistatic scattering coefficient of the composite model versus l.

4. Conclusions

To investigate the bistatic scattering interaction between the randomly Gaussian rough surface and a 2D arbitrary perfect electric conductor target, an HM combining the conventional method of moment with the KA has been developed. The approach proposed in this paper overcomes the problem of large computational requirements when using the conventional numerical methods, in which the target and rough surface in the composite model are divided into MOM region and KA region. Our method only needs to solve the EFIE in the MOM region, thus both the computational time and the memory requirements in HM are much less than that in conventional MOM. The advantage and the validity of the HM are discussed in the numerical results compared with that of MOM. Finally, the influence of the size and location of the target, the roughness parameters of the Gaussian rough surface on the bistatic scattering coefficient for different polarizations and incident angles are discussed. It must be noted that the work in this paper is just a preliminary research for the case of 1D randomly rough surface. Future investigation will include the electromagnetic scattering from the 3D arbitrary target above the 2D randomly rough surface, which is more significant in engineering, by using our HM presented in this paper.

References

[1] Guo L X and Wu Z S 2004 *J. Electromagn. Waves Appl.* **18** 1219

[2] Johnson J T 2001 *Microw. Opt. Technol. Lett.* **30** 130

[3] Pino M R, Obelleiro F, Rodriguez J L, Landesa L and Burkholder R J 2000 *IEEE Antennas and Propagation Society International Symposium* **4** 2340

[4] Colak D, Burkholder R J and Newman E H 2007 *Microw. Opt. Technol. Lett.* **49** 241

[5] Pino M R, Landesa L and Rodrigues J L 1999 *IEEE Trans. Antennas Propag.* **47** 961
[6] Pekel U, Mittra R, Ngai E, Wells T and Cohen A 1995 *IEEE Antennas and Propagation Society International Symposium* **3** 1468
[7] Pan G W 2003 *Wavelets in Electromagnetic and Device Modeling* A (New York: Wiley)
[8] Chiu T and Sarabandi K 1999 *IEEE Trans. on Antennas and Propag.* **47** 902
[9] Ye H X and Jin Y Q 2006 *IEEE Trans. Geosci. Remote Sens.* **44** 108
[10] Johnson J T 2002 *IEEE Trans. Antenna and Propag.* **50** 1361
[11] Wang Y H and Guo L X 2005 *Chin. J. Radio Sci.* **20** 580
[12] Thorsos E 1988*J. Acoust. Soc. Am.* **83** 78
[13] Jakobus U and Landstorfer F M 1995 *IEEE Trans. Antennas Propag.* **43** 162
[14] Tsang L and Kong J A 2001 *Scattering of Electromagnetic Waves* (New York: Wiley) Vol. 3 p66
[15] Harrington R F 1968 *Field Computation by Moment Methods* (Malabar, FL: Krieger)
[16] Gary A T and Thomas H N 1975 *IEEE Trans. Antennas Propag.* **23** 62
[17] Tsang L, Kong J A and Ding K H 2001 *Scattering of Electromagnetic Waves* (New York: Wiley) Vol.2 p119
[18] Ye H X and Jin Y Q 2005 *IEEE Trans. Antennas and Propag.* **53** 1234